RAPID COMMUNICATIONS

PHYSICAL REVIEW A VOLUME 51, NUMBER 3 MARCH 1995

# Observation of enhancement of stopping power and possible hydrodynamic shock behavior in penetration of large molecules in solids

Young K. Bae,* Yung Y. Chu, and Lewis Friedman
*Department of Chemistry, Brookhaven National Laboratory, Upton, New York 11973*
(Received 21 October 1994)

Measurements of the stopping power of large multiply charged ions were made by determining energy losses in thin aluminum films directly coated on solid-state detectors. With initial projectile velocities in the range of $(1–5)\times 10^7$ cm/sec, the stopping power per amu of albumin (molecular weight $M\sim 66\,290$) and cytochrome $c$ ($M\sim 12\,400$) increases quadratically in velocity to a maximum value of seven times that estimated for isolated atomic nitrogen moving with the same velocity. The observed velocity dependence of the stopping power is in qualitative agreement with the one derived from a one-dimensional shock model. Pressures estimated from the measured stopping power using the model are hundreds of megabars. The results show evidence of the collective interaction that results possibly from "hydrodynamic" shock behavior in plasmas formed by the coherent collision of high-velocity biopolymer atoms with target atoms.

PACS number(s): 79.20.Rf, 34.50.Bw, 47.40.Nm, 61.80.Mk

Impacts of large molecules and clusters at high velocities ($\geq 10^7$ cm/sec) can produce extreme conditions of transient pressure and energy density [1,2]. A hydrodynamic model predicts a pressure of $\sim 7$ Mbar and a temperature of 120 000 K, which is generated when deuterium droplets impact on a gold surface at $6\times 10^6$ cm/sec [2].

Energy densities generated by impact on and penetration of cluster ions into solid targets can be estimated from stopping power or ranges of constituent cluster atoms. Theoretical studies with Au [3] and Ag [4] clusters striking Al targets show a smaller stopping power for cluster atoms than for atomic projectiles with the same velocity. However, the theoretical analysis of low-velocity ($\sim 1\times 10^6$ cm/sec) clusters does not necessarily reflect energy transfer mechanisms with high-velocity ($>10^7$ cm/sec) projectiles. The question of interest to us was whether high-velocity clusters could compress targets with hydrodynamic shocks, which would give rise to enhanced stopping power and higher transient energy densities. These projectiles may be used to test whether there is any beam density effect on stopping power at extremely high particle-beam current densities to be used for compression and energy deposition in heavy-ion fusion.

Currently, there is no direct experimental stopping-power measurement of large clusters and molecules available. In our research on the cluster impact phenomena [5], we have discovered that the passivated solid-state detector responds to impacts of large clusters and molecules that have isolated atomic ranges up to 30 times smaller than the thickness ($\sim 500$ Å) of the boron-doped detector window. The details of these observations will be reported elsewhere [6]. Furthermore, with the electrospray ion source technique [7] which can produce large multiply charged ions, the impact energy range in our experiment has been expanded from the 600-keV limit of our Cockcroft-Walton accelerator for a singly charged ion to 30 MeV. This has facilitated direct energy-loss measurements of large molecules penetrating thin films directly coated on the detectors.

The experiments were carried out in the apparatus shown in Fig. 1. Multiply charged molecular ions were generated by an Analytica electrospray ion source modified for additional differential pumping. The details of this source can be found in Ref. [7]. Multicharged parent molecular ions, selected by a quadrupole mass analyzer were accelerated in a Cockcroft-Walton accelerator [5] to voltages as high as 600 kV. Accelerated ions were energy and mass filtered through electrostatic deflection plates and a magnetic filter [5], and then struck the detector.

Measurements of the stopping power of the large multiply charged molecules in penetration of thin films directly coated on the detectors were made by determining energy losses using Ortec Ultra solid-state detectors with 500-Å boron-doped windows. The direct coating of the films was essential. The detector did not respond with molecules through films detached from the detector, possibly because the molecules dissociated into isolated atoms before striking the detector.

Detectors were first calibrated by measuring energy deposited by the impact of ions of known kinetic energy on "bare" detector surfaces. Subsequently, the energy losses through films were directly determined from the peak shift in pulse height spectra measured with coated portions of the detectors. The detector calibration curves normalized to pulse height divided by projectile mass obtained with angiotensin (molecular weight $M\sim 1297$), cytochrome $c$ ($M\sim 12\,400$), and albumin ($M\sim 66\,290$) are presented in Fig. 2. The numbers of charges on these molecules are 3, 19, and 47, respectively. Calibration with two other detectors resulted in curves that agreed with those in Fig. 2 to within 5%. The typical detector pulse height distributions showed peaks with a full width at half maximum of $\sim 10\%$. Also shown is an extrapolated line through calibration points obtained with $\alpha$ particles (5.48 MeV) from $^{241}$Am. Most of the energy of the $\alpha$ particles is deposited in the solid detector beyond the boron-doped window. The lower-velocity atoms in the biopolymer deposit most of their energy in the boron-doped window. The lower sensitivity of detection of biopolymer atoms may reflect a limited efficiency of the window and also recombination of electrons and holes in the complex damage path of much larger projectiles.

*Present address: Phillips Laboratory/RKFE, 10 E. Saturn Blvd., Edwards AFB, CA 93524-7680.

 

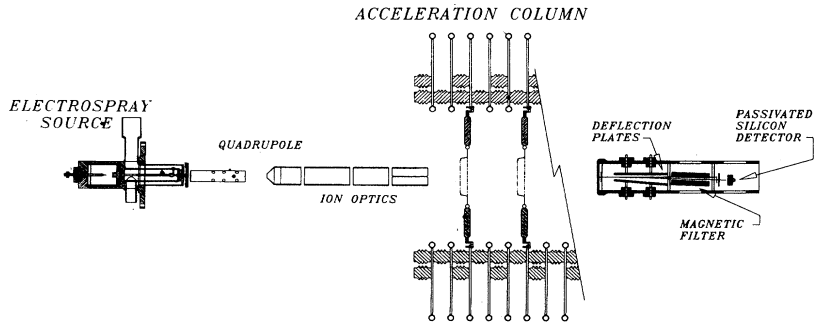


FIG. 1. Schematic diagram of the experimental apparatus.

Thin aluminum films with thicknesses of 0.5–3.0 $\mu$g/cm$^2$ were evaporated on off-centered spots on the detector. The spots were defined by a mask with apertures having diameters of 1.6 mm. The evaporation was carried out under high vacuum ($2\times10^{-7}$ Torr) by means of a Temescal electron beam source. Calibration of the film thickness was done with an XTC/2 Leybold Inficon thickness monitor with an accuracy better than 10%. The uniformity of the prepared spot could easily be checked by monitoring the detector output spectra. Nonuniform films resulted in spectra with multiple peaks. The detector chamber was pumped by an 8-in. CTI cryopump that provided an oil-free environment of a pressure of $\sim1\times10^{-7}$ Torr.

Detector pulse-height spectra obtained with albumin ions with 47 charges using a thin-film spot covered with 0.5 $\mu$g/cm$^2$ of aluminum on the detector are presented in Fig. 3. The abscissa scale, which represents the energy of the projectile entering the "bare" detector, was calculated from the calibration curve for the albumin ion in Fig. 2. The absolute magnitude of the respective peak positions subtracted from the initial projectile energies shown in the inset gave the energy losses through the thin film. For example, with 28.2-MeV albumin projectiles with an acceleration voltage of 600 kV, the detector showed approximately the energy output of 13.2 MeV, reflecting an energy loss of 15.0 MeV.

The results on energy losses through the 0.5-$\mu$g/cm$^2$ aluminum film for the angiotensin, cytochrome $c$, and albumin ions are plotted as a function of velocity in Fig. 4. The results obtained with two other detectors agreed with the data shown in Fig. 4 to within 10%. Also shown in Fig. 4 are solid lines quadratic in velocity for comparison with the experimental data. The slopes indicate that the data for cytochrome $c$ and albumin closely follow the velocity-square curves at higher velocities, but at lower velocities the data systematically deviate from the curves. The angiotensin data give a poor fit to the velocity-square curve.

Estimation of the stopping power from the measured energy losses in general assumes that the films are so thin that the energy losses are much smaller than the initial energy of the particles. However, even with the thinnest films (0.5 $\mu$g/cm$^2$) used in this work, the measured energy losses are $\sim$50% of the initial energy. Thus, exact calculation of stopping power from the measured energy losses requires the functional form of the stopping power. Since the energy losses increase quadratically in velocity (linear in energy), the stopping power should follow

$$dE/dx \sim -\alpha E, \tag{1}$$

where $\alpha$ is a constant. Then, the energy measured through a film thickness $x$ can be obtained by integrating Eq. (1) to be

$$E=E_0e^{-\alpha x}, \tag{2}$$

where $E_0$ is the initial particle energy. Once $\alpha$ is determined from the experimental data on the energy measured at various film thicknesses, the stopping power can be calculated using Eq. (1).

The energies measured through the films of various thickness of the albumin ions as a function of film thickness at the

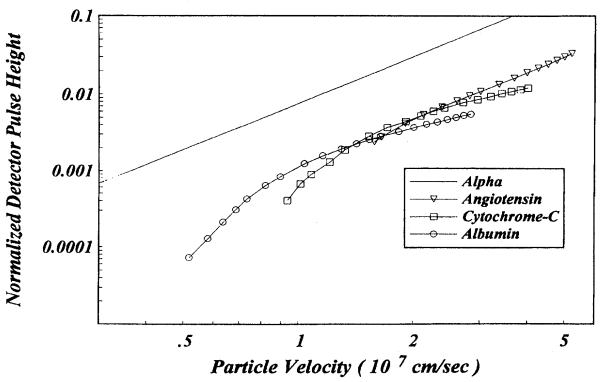


FIG. 2. "Bare" detector output pulse height divided by projectile mass as a function of the incident projectile velocity. Open circles represent data for albumin ions with $m=66\,290$ and $z=47$. Open squares represent data for cytochrome-$c$ ions with $m=12\,400$ and $z=19$. Open triangles represent data for angiotensin ions with $m=1296.5$ and $z=3$. Also shown are extrapolated calibration data of 5.48-MeV $\alpha$ from $^{241}$Am.

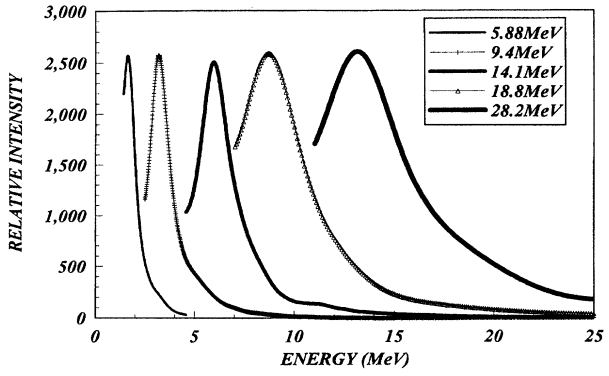


FIG. 3. Detector pulse height spectra of albumin ions accelerated at 5.88–28.2 MeV through the 0.5-$\mu$g/cm$^2$ aluminum film coating the detector. The magnitude of the energy shift from the incident projectile energy shown in the inset gives the energy loss.

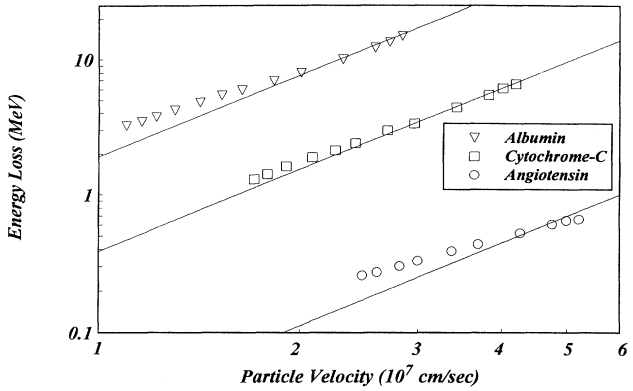


FIG. 4. Energy losses through a 0.5-$\mu$g/cm$^2$ aluminum film. Open-triangle data were obtained with albumin ions with $m=66\,290$ and $z=47$. Open-square data were obtained with cytochrome-$c$ ions with $m=12\,400$, $z=19$. Open-circle data were obtained with angiotensin ions with $m=1296.5$ and $z=3$. The solid curves are quadratic in velocity for comparison with the data.

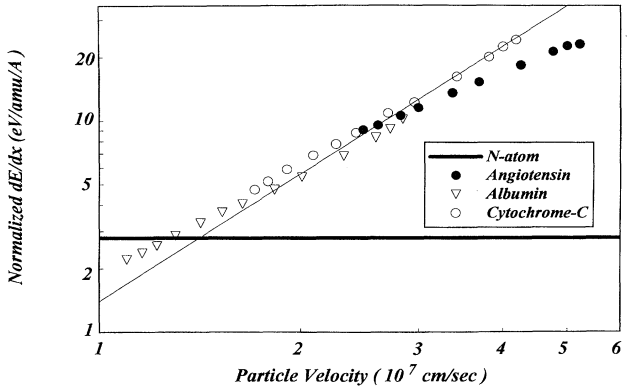


FIG. 6. Normalized stopping power of various molecules as a function of velocity in units of eV/Å/amu. Open-triangle data are for albumin ions with $M=66\,290$ and $z=47$. Open-circle data are for cytochrome-$c$ ions with $M=12\,400$ and $z=19$. The closed-circle data are for angiotensin ions with $M=1269.5$ and $z=3$. The solid curve represents the calculated normalized stopping power per amu of N atoms from the mean range curve of Ziegler *et al.* [8].

initial projectile energy of 23.5 MeV are shown as a semi-log plot in Fig. 5. The data decrease approximately exponentially with increasing film thickness, in agreement with Eq. (2). This agreement is additional evidence for the velocity-square dependence of the stopping power of the molecules. A curve fitting of the data to Eq. (2) with $E_0=23.5$ MeV resulted in $\alpha=0.0235$ and $dE/dx=0.55$ MeV/Å. The fitting results were then used for converting energy-loss data to stopping power. Because the angiotensin data poorly follow the velocity-square curve (Fig. 3), the above procedure should give larger errors, which are estimated to be 20–30 % in the stopping power for angiotensin.

To compare the stopping power of different molecular species, we normalized the stopping power by dividing it by the corresponding molecular mass. The normalized stopping powers in units of eV/(Å amu) for the angiotensin, cytochrome $c$, and albumin ions are plotted as a function of velocity in Fig. 6. Because the constituent heavy atoms that carry most of the energy of these protein molecules are C, N, and O, the energy loss based on the isolated atomic energy losses of the molecules can be roughly calculated from the energy losses of N atoms. Thus, a thick solid curve for the normalized N-atom stopping power per amu calculated from the mean range curve of Ziegler, Biersack, and Littmark *et al.* [8] is also included. The flat N-atom curve reflects the compensation in energy dependence of the nuclear and electronic stopping power over the range of velocity. Also shown in Fig. 6 is a solid curve obtained by fitting both albumin and cytochrome-$c$ data to a velocity-square curve.

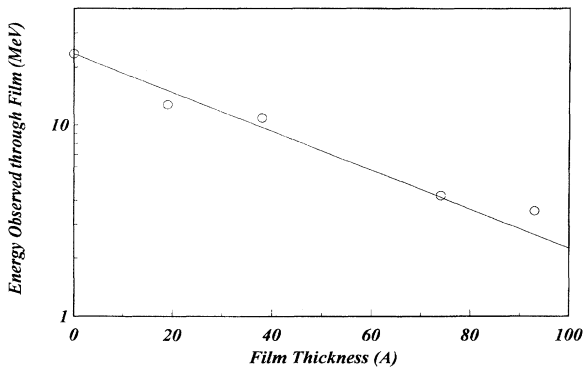


FIG. 5. Energy measured through the films as a function of film thickness. The data were obtained with albumin ions ($M=66\,290$ and $z=47$) at the initial projectile energy of 23.5 MeV. The solid curve resulted from curve fitting the data to Eq. (2).

The albumin and cytochrome-$c$ data show an approximately quadratic increase in velocity and fall within a narrow band around the velocity-square curve. However, angiotensin data systematically deviate away from the velocity-square curve with increasing velocity. With angiotensin, the projectile size ($\sim 100$ atoms) may be approaching the vicinity of the critical threshold of transition from micro to macro projectiles. The stopping power of cytochrome $c$ at the highest available velocity is approximately a factor of 7 larger than the normalized N-atom stopping power. With the results for albumin at the lower velocities, the normalized $dE/dx$ values are smaller than the stopping power of atomic nitrogen.

Particularly, the velocity-square dependence of the stopping power may reflect the development of the hydrodynamic shock behavior. Let us think about a simple one-dimensional system in which the projectile with a cross-sectional area $A$ impacts a disk with a thickness $\Delta x$ and an area $A$. Our model assumes the development of a shock wave prior to any appreciable penetration by the projectile into the target. Also, we assume that the projectile loses its energy mostly in producing a shock wave and that the shocked material behaves almost like a monoatomic gas, with $\gamma=\frac{5}{3}$, as in the case of very strong shocks [9]. Under these assumptions, the energy deposited in the disk is given by

$$\Delta E \sim (dE/dx)\Delta x, \tag{3}$$

where $dE/dx$ is the stopping power of the projectile. The energy stored in the disk after compression [9] is given by

$$\Delta E \sim \tfrac{3}{2}PV, \tag{4}$$

where $P$ and $V$ are the pressure and the volume after compression, respectively.

Following Zel'dovich and Raizer [9], if the target density $\rho_T$ is much greater than the projectile density $\rho_P$, before

collision the pressure $P_s$ and the density $\rho_s$ of the shocked target material in the one-dimensional shock produced by the impact of particles at a velocity $v_0$ are

$$P_s \sim \tfrac{4}{3}\rho_P v_0^2, \tag{5}$$

$$\rho_S = 4\rho_T. \tag{6}$$

Thus, the volume $V$ of the disk after compression is

$$V \sim A\Delta x/4. \tag{7}$$

Combining Eqs. (3), (4), and (7) results in

$$P \sim (8/3A)(dE/dx), \tag{8}$$

$$dE/dx \sim (A/2)\rho_P v_0^2. \tag{9}$$

Therefore, our simple model qualitatively shows that the stopping power of the particles, the impact of which can develop shock waves, should follow the velocity-square dependence.

With the use of Eq. (8), the shock pressures produced by the impact of the molecules and clusters can be estimated. The estimated pressures produced by the impact of the albumin and cytocrome-*c* ions at maximum available velocities ($v \sim 2.8\times 10^7$ cm/sec for albumin and $v \sim 4.2\times 10^7$ cm/sec for cytochrome *c*) are $\sim$200 and $\sim$300 Mbar, respectively. In this estimation, the cross-sectional areas of the albumin (15 000 Å$^2$) and cytochrome-*c* (4200 Å$^2$) ions were obtained from the collisional cross sections measured by Covey and Douglas [10]. On the other hand, the use of Eq. (5) for estimating pressures for albumin and cytochrome *c* resulted in lower values: $\sim$60 Mbar for albumin and $\sim$180 Mbar for cytochrome *c*. Perhaps more rigorous models would resolve the discrepancy between the pressures estimated from Eqs. (5) and (8).

If our shock model is correct, it appears that large molecules that are accelerated to velocities greater than 100 km/sec can generate pressures on the order of hundreds of megabars. Also our technique demonstrates that extreme pressure over hundreds of megabars generated by particle impact can be directly measured using silicon particle detectors. With a factor of 7 enhancement in stopping power observed in these experiments and a factor of 4 increase in particle density [Eq. (6)], the transient energy densities produced by cluster impact after compression at the maximum velocity available in these experiments are roughly 30 times the values estimated for isolated atomic projectiles.

The enhanced stopping power of large clusters suggests possible additional advantages in the generation of very high energy density assemblies for this purpose. We note that at velocities smaller than the Fermi velocity, $v_F \sim 3\times 10^8$ cm/sec, isolated atomic stopping processes involve mainly electronic energy transfer, and $dE/dx$ increases linearly with projectile velocity [8]. At higher velocities greater than $v_F$, atomic stopping curves over and decreases with velocity [8]. The interesting question is whether $dE/dx$ for cluster projectiles will continue to follow the dependence on the square of the projectile velocity with higher velocities and to what extent the enhanced stopping power can be increased. If the velocity-square dependence persists at higher velocities, the energy density achieved by molecule and cluster impact can be many orders of magnitude greater than that achieved by isolated atomic projectiles. The high-energy density can be very useful for enhancing the efficiency of heavy-ion fusion [11].

The fundamental difference between energy loss via the hydrodynamic model and from isolated penetrating atomic projectiles is that with the former a shock wave is developed at the surface of impact and energy is absorbed with the compression of target and projectile atoms. For this to account for a significant fraction of projectile energy, the projectile atoms must slow down at the impact surface at a much more rapid rate than with penetrating projectiles. Otherwise, projectile atoms penetrate the target with a relatively minor loss of energy.

Secondary electron yield studies show that energetic clusters can excite thousands of electrons in a very small target surface element [12]. If clusters with sufficiently high velocity initially produce very hot dense plasmas at the target surface, than the screened Coulomb potentials used to describe nuclear stopping processes may be perturbed. Much stronger repulsive interactions between projectile and target nuclei can give rise to a more rapid slowing down of projectile atoms. The nature of such dense energetic plasmas and rates of energy transfer between target and projectile atoms under these transient extreme conditions presents a fertile area for theoretical [13,14] and further experimental research.

The invaluable technical contributions of Y. Xu, R. J. Beuhler, S. Howell, E. Ritter, J. G. Alessi, and V. LoDestro are gratefully acknowledged. We also thank G. Friedlander for stimulating discussions. This research was carried out at Brookhaven National Laboratory under Contract No. DE-AC0276CH00016 with the U.S. Department of Energy and supported by its Advanced Energy Projects and Division of Chemical Sciences, Office of Basic Energy Sciences.

[1] F. Winterberg, Z. Naturforsch. A **190**, 231 (1964).
[2] L. Friedman and G. H. Vineyard, Comments At. Mol. Phys. **15**, 251 (1984).
[3] V. I. Shulga and P. Sigmund, Nucl. Instrum. Methods B **47**, 236 (1990).
[4] Y. Yamamura and T. Muramoto, Phys. Rev. Lett. **69**, 1463 (1992).
[5] Y. K. Bae *et al.*, Phys. Rev. A **48**, 4461 (1993).
[6] Y. K. Bae,, R. Beuhler, Y. Y. Chu, G. Friedlander, Y. Xu, and L. Friedman (unpublished).
[7] J. B. Fenn *et al.*, Science **246**, 64 (1989).
[8] J. F. Ziegler *et al.*, *The Stopping and Range of Ions in Solid* (Pergamon, New York, 1985), Vol. 1.
[9] Y. B. Zel'dovich and Y. P. Raizer, *Physics of Shock Waves and High-Temperature Hydrodynamic Phenomena* (Academic, New York, 1966).
[10] T. Covey and D. J. Douglas, Am. Soc. Mass Spec. **4**, 616 (1993).
[11] C. Deutch and N. A. Tahir, Phys. Fluids B **4**, 3735 (1992).
[12] Y. Xu *et al.*, J. Phys. Chem. **97**, 11 883 (1993); J. Axelsson *et al.*, Nucl. Instrum. Methods B **88**, 131 (1994).
[13] S. M. Younger *et al.*, Phys. Rev. Lett. **61**, 962 (1988).
[14] M. H. Shapiro *et al.*, Nucl. Instrum. Methods B **88**, 81 (1994).